ACS EARTH AND SPACE CHEMISTRY

http://pubs.acs.org/journal/aesccq

Article

Distribution Coefficients of the REEs, Sr, Y, Ba, Th, and U between α-HIBA and AG50W-X8 Resin

Haoyu Li, François L. H. Tissot,* Seung-Gu Lee, Eugenia Hyung, and Nicolas Dauphas

Cite This: ACS Earth Space Chem. 2021, 5, 55−65

Read Online

ACCESS | Metrics & More | Article Recommendations | Supporting Information

ABSTRACT: Rare-earth elements (REEs) are known for their similar behaviors, which make their purification through chromatographic techniques particularly challenging. The use of α-hydroxyisobutyric acid (α-HIBA) in combination with a cation-exchange resin is perhaps the most widely used chromatographic technique to separate individual REEs from each other. However, only limited REE partition data between α-HIBA and cation resins exist, which makes it challenging to develop and optimize purification techniques using this platform. Here, we report distribution coefficients (K_d) of REEs, as well as Sr, Y, Ba, Th, and U, between α-HIBA at pH = 4.50 and AG50W-X8 cation-exchange resin, obtained by batch equilibration experiments. For all 19 elements, the distribution coefficients decrease with increasing acid concentration. For the REEs, a linear relationship is observed in log−log space between K_d values and α-HIBA molarity. While the K_d values have been calibrated at pH = 4.50, formulas are provided allowing recasting of the K_d values at any pH. To test the accuracy of the data, we compare elution curves simulated using the newly determined distribution coefficients to actual elution curves. The close agreement between simulated and experimental elution curves demonstrates that the distribution coefficients obtained in this study are effective to devise multielement extraction and purification scheme for high-precision elemental and isotopic analyses of REEs for various applications.

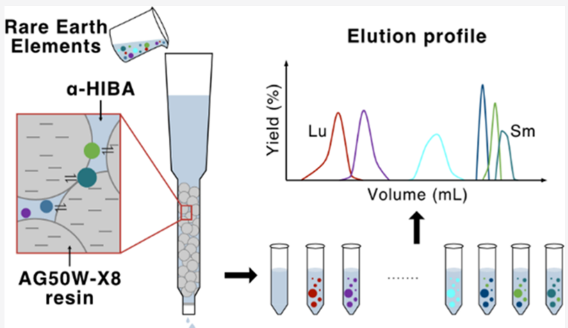

KEYWORDS: *distribution coefficients, extraction chromatography, REEs, α-HIBA, AG50W-X8 resin*

1. INTRODUCTION

The characterization of isotopic variations for the rare-earth elements (REEs) has found diverse applications in the fields of geo- and cosmochemistry.[1−14] For instance, the Sm−Nd decay system, which is arguably the best-known and most-studied of the REE systematics, contains two radiogenic isotopes (^{147}Sm → ^{143}Nd, $t_{1/2}$ = 106 Byr;[15] ^{146}Sm → ^{142}Nd, $t_{1/2}$ = 103 Myr[16]) which are widely used in (i) geochronology,[17,18] (ii) the tracing of mantle sources,[19,20] and (iii) the study of the differentiation history of planetary silicate reservoirs.[2,21−23] In cosmochemistry, Nd nucleosynthetic anomalies have recently proven to be critical to our understanding of planetary formation and early solar-system dynamics.[3,4,24] In recent years, high-precision isotopic investigations of other REE systematics have also been pioneered (*e.g.*, Ce, Eu, Dy, Er, and Yb isotopes)[5,25−28] as new possible tools to solve geo- and cosmochemical questions,[5,29,30] revealing a growing need for robust purification protocols for all REEs.

Geochemically, REEs are well known for their near identical behavior, which stems from (i) their very similar ionic radii, and (ii) the fact that most of these metal ions exist primarily in the trivalent oxidation state in geological samples (Eu and Ce can also exist as Eu^{2+} and Ce^{4+}, respectively). These characteristics make the separation of REEs especially difficult.[31] As the most well-studied REE isotope system, methods for separating Sm and Nd[2,23,32−39] are well established. To a lesser extent, routine protocols also exist for Lu (part of the Lu−Hf system),[40−44] Ce (part of the La−Ce system),[28,45−49] and Sm/Gd (for characterization of cosmogenic effects).[50−54] For high-precision isotopic investigations of other REE systems, optimized methods are not yet readily available.

To streamline the development and optimization of REE purification protocols, knowledge of the partition behavior of the elements of interest between the eluent and the resin is necessary. The affinity of a resin for a particular element is given by a distribution coefficient, K_d, which quantifies the partitioning of the element between the eluent (mobile phase) and the extractant (stationary phase) and is defined as

$$K_d = C_s/C_l \quad (1)$$

where C_s is the concentration of the element exchanged with the resin, in μg per gram of dry resin, and C_l is the concentration of the element remaining in the solution after the equilibrium has

Received: October 1, 2020
Revised: December 2, 2020
Accepted: December 2, 2020
Published: December 15, 2020

been achieved between the mobile and the stationary phases, in μg per mL of solution. For REEs, one of the most widely used separation techniques is the α-hydroxyisobutyric acid (α-HIBA) ion-exchange chemistry,[10,18,32,34,55−72] in which the eluent is the α-HIBA, $(CH_3)_2$−COH−COOH, and the stationary phase is the AG50W-X8 strong cation-exchange resin. α-HIBA is a weak acid with a pK_a ($pK_a = -\log_{10}(K_a)$, where K_a is the acid dissociation constant) of 3.79. Despite its popularity, a dearth of distribution coefficient data exists for this particular eluent/resin combination, making calibrations of REE separation an unnecessarily lengthy process of trial and errors.

Here, we report the determination of distribution coefficients of the REEs, as well as Sr, Y, Ba, Th, and U between α-HIBA at pH = 4.50 (±0.01) and the AG50W-X8 resin over a range of molarities from 0.010 to 2.123 M α-HIBA. Although the REEs are the focus of this paper, Sr, Ba, Y, Th, and U were also investigated to better assess how similar their partition behavior is compared to REEs during the α-HIBA chemistry[73,74] and should separation of these elements be necessary to avoid matrix effects. While these K_d values have been calibrated at pH = 4.50, formulas are provided allowing recasting of the REEs K_d values at any pH. To test the accuracy of the REE distribution coefficients, we compare simulated elution profiles to both coarse (used for concentration determinations) and fine (used for high-precision isotopic analyses) experimentally determined elution curves.

2. EXPERIMENTAL SECTION

2.1. Reagents and Analytical Materials. AG50W-X8 resin (200−400 mesh, hydrogen form) was purchased from Bio-Rad, and α-HIBA from Alfa Aesar, as 2-hydroxyisobutyric acid (99% dry wt, molar mass 104.11 g/mol). Other acids used in this work (HCl, HNO_3) were procured at the analytical grade and double distilled in quartz and/or PTFE Teflon distillation units (PicoTrace at University of Chicago; Savillex at Caltech). Milli-Q water (Millipore, resistivity > 18.2 MΩ/cm) was used for cleaning, acid dilutions, and chromatography. All Teflon labware were precleaned with successive leaching in boiling nitric acid and aqua regia. All chemical treatments in this study were performed inside a clean laboratory environment, at room temperature.

2.2. Preparation of α-HIBA Solutions. For K_d batch experiments, the α-HIBA stock solution was prepared in glassware precleaned by rinsing in 10% vol HCl, followed by overnight immersion in 6 M HCl on a hot plate. α-HIBA powder weighing 208.30 g was dissolved in 650 mL of Milli-Q (hereafter, MQ) water and left to react for 2 h, after which the solution was filtered to remove any nondissolved acid particles. For reference, the solubility of α-HIBA in water is 484 g/L. Filtration took 6 h and was done with a PTFE-faced funnel, base glass filter holder, and 0.45 μm Fluoropore hydrophobic PTFE membranes (Millipore), prewetted with alcohol. The pH of the filtered solution was adjusted to 4.50 by the addition of 95 mL NH_4OH (ammonium hydroxide; $pK_b = 4.77$, $pK_b = -\log_{10}(K_b)$, where K_b is the base dissociation constant) solution. The pH-adjusted solution (718.48 g) was transferred into a triple-cleaned Teflon bottle and diluted with MQ-water to a final weight of 1000.04 g, corresponding to an α-HIBA concentration in the final solution of ∼2.123 M.

For the elution conducted at Caltech (Elution 2 in Discussion), a 0.2 M α-HIBA stock solution was prepared by adding MQ-water to 41.64 g of α-HIBA powder in a graduated cylinder until the solution volume added up to 2.00 L. The pH of the 0.2 M α-HIBA solution was subsequently adjusted to 4.62 by adding ∼36 mL of Optima-grade NH_4OH.

2.3. Batch Equilibration Experiment. Distribution coefficients were determined through batch equilibration of the elements of interest in various molarities of the α-HIBA solution. From the α-HIBA stock solution (2.123 M), twenty-four dilutions were prepared covering the molarities between 0.010 and 1.064 M. A multielement mixture containing the 14 REEs, as well as Sr, Y, Ba, Th, and U, was prepared by adding ∼3.6 g of single-element inductively coupled plasma mass spectrometry (ICP−MS) standard solutions (each 1000 ± 5 ppm, SPEX CertiPrep). These solutions are available in a combination of dilute HF, H_2O_2, HCl, and/or HNO_3. If present in solution during the batch equilibration, even trace amounts of these reagents could potentially modify the partitioning of elements between the resin and solution. To avoid such complications, aliquots of standard solutions were transferred to a precleaned Teflon beaker and evaporated to dryness. Right before complete evaporation, the residual droplet was taken back into 5 mL of 3 M HNO_3, transferred to a clean centrifuge tube, and diluted with MQ-water to 50 mL (0.3 M HNO_3). Remaining insoluble particles were removed by centrifugation, after which an aliquot of the multielement standard solution was sampled, diluted, and analyzed by MC−ICPMS. All elements added to the standard were detected at levels of at least three orders of magnitude above blank 0.3 M HNO_3 solutions, and the concentrations of each element in the multielement solution were ∼72 ppm.

The AG50W-X8 resin was precleaned and converted to ammonium form in a 1 L Teflon column with MQ-water (3 column volume; cv), followed by a 6 M HCl rinse (3 cv) and another MQ water rinse (3 cv). The resin was then transferred to a triple cleaned Teflon bottle, soaked in 1 M NH_4OH for 1 h, rinsed with MQ-water (2 cv), and finally soaked in MQ-water (*i.e.*, neutral pH, ammonium form).

The protocols for the equilibration experiments were modified from those described in ref 75. Batch experiments were conducted in α-HIBA solution ranging from 0.010 to 2.123 M. For each molarity, 4.7 mL of cleaned resin (equivalent to 2 g of dry mass) was pipetted into a precleaned Teflon beaker and dried on a hot plate at ∼60 °C to remove the water remaining in the resin. Then, 10 mL of α-HIBA solution at the adequate molarity for the equilibration was added to the beakers and left to equilibrate overnight to convert the resin to the α-HIBA form. The solution was then pipetted out, and the beakers were placed in a blowing hood to dry the resin. In another clean Teflon beaker, the molarity specific standard solution was prepared by adding 0.2 mL of the ∼72 ppm multielement standard solution (0.3 M HNO_3) into 7 mL α-HIBA solution at the chosen molarity (0.010−2.123 M α-HIBA). A 1 mL aliquot of the solution was saved and used as a standard for concentration normalization. The remainder of the molarity-specific standard solution (6 mL, containing ∼12.4 μg of each element of interest) was added to the resin, resulting in an element to resin ratio of ∼6.2 μg/g. The resin and the acid-standard solutions were stirred by placing the beakers on a Thermolyne Vortex shaker (1000 rpm) for 5−10 min every 2 h. After 8 h of equilibration, the mixture was filtered using precleaned Bio-Rad Poly-Prep chromatography columns, to separate the resin from the mobile phase. The acid solutions were collected in centrifuge tubes and transferred back into cleaned Teflon beakers. The equilibrated solutions (hereafter "sample") and the nonequilibrated aliquots (hereafter "standard") were dried on a hot plate and taken back

https://dx.doi.org/10.1021/acsearthspacechem.0c00273
ACS Earth Space Chem. 2021, 5, 55−65

Table 1. Faraday Cup Configuration Used for REE Concentration Measurements on the MC−ICPMS[a]

configuration	L4	L3	L2	L1	axial	H1	H2	H3	H4
main	^{149}Sm	^{151}Eu	^{157}Gd		^{159}Tb	^{163}Dy		^{165}Ho	^{167}Er
sub sequence 1			^{139}La	^{140}Ce	^{141}Pr		^{146}Nd		
sub sequence 2			^{167}Er		^{169}Tm	^{173}Yb		^{175}Lu	
sub sequence 3					^{88}Sr				
sub sequence 4					^{89}Y				
sub sequence 5					^{138}Ba				
sub sequence 6					^{232}Th				
sub sequence 7					^{238}U				

[a] ^{167}Er was measured twice: in the main sequence and in subsequence 2. The results from these two measurements agreed with each other within error, so distribution coefficients of Er were calculated as the mean of the two measurements.

into 5 mL of 0.3 M HNO_3. For each "sample" and "standard", an aliquot was taken and diluted 20-fold to achieve concentrations of at most ~100 ppb for an element that would have remained entirely in the liquid phase during the equilibration experiment.

2.4. Mass Spectrometry. Concentration measurements on the diluted "sample" and "standard" solutions were performed on a Thermo Finnigan Neptune MC−ICPMS at the Origins Lab, following a protocol modified from ref 76. In brief, the 14 REEs were measured using 3 cup subconfigurations with ^{159}Tb, ^{141}Pr, and ^{169}Tm on the axial Faraday cup, respectively. Then, ^{88}Sr, ^{89}Y, ^{138}Ba, ^{232}Th, and ^{238}U were measured in the center cup, in five successive subconfigurations (*i.e.*, peak jumping) (Table 1). Measured isotopes were selected with preference given to higher relative abundances and absence of isobaric/polyatomic interferences. The 0.3 M HNO_3 solutions were introduced into the MC−ICPMS using a 100 μL/min PFA Teflon self-aspirating nebulizer. Measurements were performed in wet plasma mode, using a combined quartz cyclonic and Scott-type spray chamber (Stable Introduction System from ESI). Instrumental drift was corrected for by bracketing every batch of three unknowns with a multielement standard solution (std−smp−smp−smp−std). The procedural blank and acid contributions (generally < 1%) were subtracted from each analysis.

For the elution conducted at Caltech (Elution 2), concentration in each elution cut was measured using an iCAP RQ (Thermo Fisher) ICP−MS and an SC-2 DX autosampler (Elemental Scientific). Instrumental tuning parameters (*e.g.*, nebulizer gas flow, torch alignment, sample uptake rate, and quadrupole ion deflector) were optimized to pass the standard performance check using an iCAP Q/RQ solution (Thermo Fisher Scientific) containing 1.0 ppb Ba, Bi, Ce, Co, In, Li, and U in 2% HNO_3 and 0.5% HCl. After tuning, REE standard solutions covering a range of concentrations were measured to generate calibration curves that establish the signal to concentration correspondence (*i.e.*, counts per second per ppm) for the analytical session. Analyses were conducted in the STD mode. The typical signal variability from instrumental drift in these conditions is around ±1% within any given session.

2.5. Elution Tests. We conducted two elution tests to assess the accuracy of the distribution coefficients obtained from the batch equilibration experiments. Matrix elements were omitted in the artificial solution used in these tests as REE separation are typically performed on a preconcentrated REE fraction after removal of matrix elements in the sample.

Elution 1 was conducted at the Origins Lab (University of Chicago) at room temperature by using a custom-made quartz column (1.9 mm ID × 21 cm length) to achieve a bulk separation for concentration measurements. A multielement standard solution containing 10 ppm of each REE was loaded on the column filled with AG50W-X8 resin (200−400 mesh) in 1 mL 0.06 M α-HIBA. Lu, Yb, and Tm were eluted with 36 mL of 0.06 M α-HIBA, followed by Er, Eu, Sm, and Nd in 16 mL of 0.2 M α-HIBA and finally Pr and Ce in 10 mL of 0.3 M α-HIBA. The concentration measurements were performed with the same experimental setup as the distribution coefficient measurements, and the yield for each REE was above 90%.

Elution 2 was conducted at the Isotoparium (Caltech) with a borosilicate column (2.0 mm ID × 30 cm length) at ambient temperature and pressurized to 1.0 psi (frit porosity: 35 μm) using compressed air, which produces a fine separation of Ce−Nd−Sm for high-precision isotopic analysis of Nd. The flow rate was 1 drop/min, and each elution fraction consisted of four drops (~47 μL/drop). A standard mixture with 60 ppm of each REE was loaded on the column filled with AG50W-X4 resin (200−400 mesh) in 150 μL of 0.75 M HCl, and an isocratic elution was done with 8.3 mL of 0.2 M α-HIBA at a pH of 4.62. Elution fractions were collected in four drop increments in 5 mL Teflon vials, dried down at 90 °C, and redissolved into 0.48 M HNO_3. Concentrations were measured on the iCAP RQ ICP−MS, and yields for all REEs were above 90%.

2.6. Elution Simulations. To simulate the elutions, we used an optimized (~18× faster) version of the Mathematica code from ref 77, which is based on the plate theory of chromatography developed by Martin and Synge.[78] The plate theory states that a chromatographic column can be divided into a finite number of theoretical plates of defined height (noted HETP, for height equivalent to a theoretical plate). Within each plate, and at any point in time, equilibrium is achieved between the liquid (mobile) phase and the solid (stationary) phase. Using this framework, it is possible to model the behavior of elements onto a resin and test various elution schemes to optimize the separation of the elements of interest. The architecture of the simulation code is summarized in Table S1. This simulation code (Supporting Information) allows users to model the behavior of elements onto a specific resin and rapidly test complex elution schemes to optimize the separation of the elements of interest prior to implementation in the laboratory. Sensitivity tests were performed to evaluate the influence of uncertainties on parameters such as column dimensions (*i.e.*, length and radius) and resin properties (*i.e.*, porosity and density) (Figure S1). Within the accuracy of typical determination of these parameters, they do not influence the results of the simulations presented here.

Table 2. Distribution Coefficients (K_d) of REEs, Sr, Y, Ba, Th, and U, at pH = 4.50[a,b]

α-HIBA (M)	Sr	Y	Ba	La	Ce	Pr	Nd	Sm	Eu	Gd	Gd *	Tb	Dy	Ho	Er	Tm	Yb	Lu	Th	U
0.010	10,142	**	8028	**	**	**	**	**	**	**	**	**	**	**	**	**	**	**	**	8976
0.016	8773	**	18,913	**	**	**	**	**	**	**	**	**	**	**	**	**	**	**	20,747	3209
0.026	7905	19,518	15,363	**	**	**	**	**	**	**	**	**	**	**	21,606	13,422	7938	5754	2736	497
0.041	6630	4708	13,846	**	**	**	**	**	**	31,265	21,224	12,155	6290	3760	2109	1248	745	517	206	116
0.063	4616	420	9876	**	**	28,858	19,439	7007	3701	3770	2235	995	488	285	159	91.6	53.7	36.0	18.5	27.1
0.083	2990	62.5	7519	22,221	9983	5741	3774	1144	601	612	521	148	71.0	40.7	22.3	12.8	*	*	*	*
0.107	2706	22.6	7424	10,098	4117	2347	1519	433	222	226	131	53.3	25.9	15.1	*	*	*	*	*	*
0.135	2384	*	6717	3995	1556	895	577	159	80.6	84.9	39.0	19.9	10.3	*	*	*	*	*	*	*
0.160	1733	*	4791	1407	540	313	202	54.6	27.8	30.9	15.9	*	*	*	*	*	*	*	*	*
0.187	1220	*	3448	570	217	126	81.0	21.7	10.9	13.2	*	*	*	*	*	*	*	*	*	*
0.214	1034	*	2756	214	82.5	46.7	29.9	*	*	*	*	*	*	*	*	*	*	*	*	*
0.241	1153	*	2975	256	98.6	56.3	36.1	*	*	*	*	*	*	*	*	*	*	*	*	*
0.267	780	*	650	114	44.0	25.0	15.9	*	*	*	*	*	*	*	*	*	*	*	*	*
0.293	668	*	1658	79.3	30.8	17.6	11.2	*	*	*	*	*	*	*	*	*	*	*	*	*
0.321	502	*	1154	37.6	14.8	*	*	*	*	*	*	*	*	*	*	*	*	*	*	*
0.348	576	*	1331	37.5	15.8	*	*	*	*	*	*	*	*	*	*	*	*	*	*	*
0.375	312	*	729	15.5	*	*	*	*	*	*	*	*	*	*	*	*	*	*	*	*
0.403	345	*	768	14.3	*	*	*	*	*	*	*	*	*	*	*	*	*	*	*	*
0.426	259	*	584	*	*	*	*	*	*	*	*	*	*	*	*	*	*	*	*	*
0.533	164	*	393	*	*	*	*	*	*	*	*	*	*	*	*	*	*	*	*	*
0.691	102	*	275	*	*	*	*	*	*	*	*	*	*	*	*	*	*	*	*	*
0.849	52.2	*	156	*	*	*	*	*	*	*	*	*	*	*	*	*	*	*	*	*
1.064	32.0	*	106	*	*	*	*	*	*	*	*	*	*	*	*	*	*	*	*	*
2.123	*	*	21.8	*	*	*	*	*	*	*	*	*	*	*	*	*	*	*	*	*

[a]For distribution coefficients, * denotes values smaller than 10 and ** values larger than $10^{4.5}$. [b]Gd* represents the corrected distribution coefficients of Gd (recommended value, see text for details).

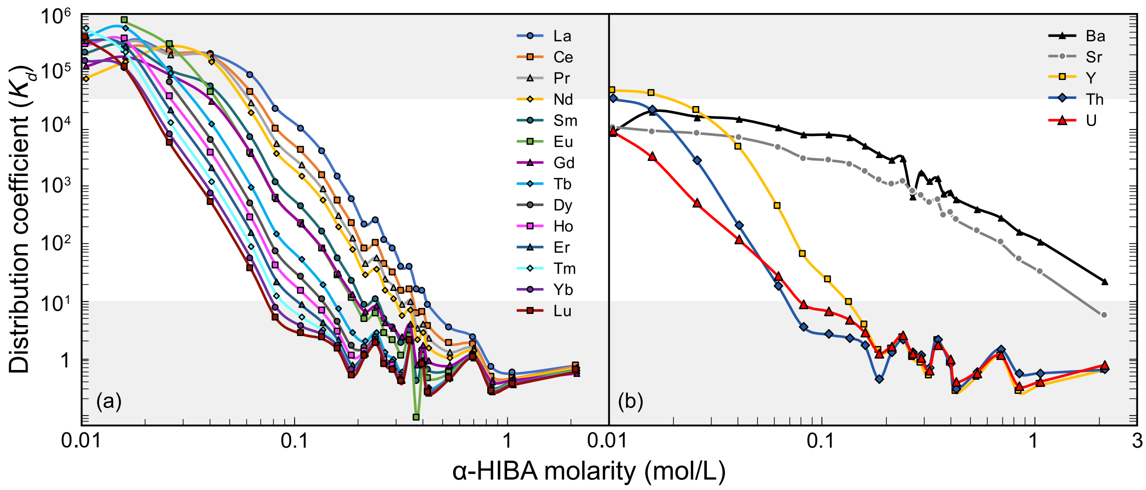

Figure 1. Distribution coefficients of (a) REEs and (b) Ba, Sr, Y, Th, and U on AG50W-X8 resin as a function of α-HIBA molarity. Only values within the $10 < K_d < 10^{4.5}$ range are considered reliable and reported in Table 2. For $K_d < 10$ (lower grey band), insufficient change in the solution concentrations occurred, while above $10^{4.5}$ (upper grey band), the analyte concentrations approached the limits of detection of the instrument.

Table 3. Linear Regression Statistics for Determination of REE K_d as a Function of α-HIBA Molarity[a]

element	equation	r^2
La	$\log_{10}(K_d) = -(4.83 \pm 0.30)\ [\log_{10}([\text{HIBA}]) + \text{pH-}4.50] - (0.73 \pm 0.21)$	0.989
Ce	$\log_{10}(K_d) = -(4.77 \pm 0.35)\ [\log_{10}([\text{HIBA}]) + \text{pH-}4.50] - (1.08 \pm 0.25)$	0.988
Pr	$\log_{10}(K_d) = -(4.81 \pm 0.32)\ [\log_{10}([\text{HIBA}]) + \text{pH-}4.50] - (1.35 \pm 0.26)$	0.991
Nd	$\log_{10}(K_d) = -(4.84 \pm 0.32)\ [\log_{10}([\text{HIBA}]) + \text{pH-}4.50] - (1.56 \pm 0.27)$	0.991
Sm	$\log_{10}(K_d) = -(5.07 \pm 0.45)\ [\log_{10}([\text{HIBA}]) + \text{pH-}4.50] - (2.30 \pm 0.43)$	0.992
Eu	$\log_{10}(K_d) = -(5.11 \pm 0.44)\ [\log_{10}([\text{HIBA}]) + \text{pH-}4.50] - (2.63 \pm 0.42)$	0.993
Gd	$\log_{10}(K_d) = -(5.05 \pm 0.27)\ [\log_{10}([\text{HIBA}]) + \text{pH-}4.50] - (2.54 \pm 0.27)$	0.997
Gd*	$\log_{10}(K_d) = -5.28\ [\log_{10}([\text{HIBA}]) + \text{pH-}4.50] - 3.00$	
Tb	$\log_{10}(K_d) = -(5.44 \pm 0.64)\ [\log_{10}([\text{HIBA}]) + \text{pH-}4.50] - (3.54 \pm 0.71)$	0.990
Dy	$\log_{10}(K_d) = -(5.45 \pm 0.72)\ [\log_{10}([\text{HIBA}]) + \text{pH-}4.50] - (3.85 \pm 0.80)$	0.987
Ho	$\log_{10}(K_d) = -(5.88 \pm 0.79)\ [\log_{10}([\text{HIBA}]) + \text{pH-}4.50] - (4.61 \pm 0.93)$	0.991
Er	$\log_{10}(K_d) = -(5.92 \pm 0.56)\ [\log_{10}([\text{HIBA}]) + \text{pH-}4.50] - (4.98 \pm 0.75)$	0.996
Tm	$\log_{10}(K_d) = -(5.99 \pm 0.54)\ [\log_{10}([\text{HIBA}]) + \text{pH-}4.50] - (5.30 \pm 0.72)$	0.996
Yb	$\log_{10}(K_d) = -(5.67 \pm 0.55)\ [\log_{10}([\text{HIBA}]) + \text{pH-}4.50] - (5.05 \pm 0.77)$	0.998
Lu	$\log_{10}(K_d) = -(5.76 \pm 0.54)\ [\log_{10}([\text{HIBA}]) + \text{pH-}4.50] - (5.33 \pm 0.76)$	0.998

[a] Uncertainties of slope and y-intercept are reported as two standard errors. Gd* represents the corrected regression statistics of Gd (recommended value, see text for details).

3. RESULTS

3.1. Distribution Coefficients. To calculate the distribution coefficients for each element (*i.e.*, μg of element per g of resin divided by μg of element per mL of solution), an extended form of eq 1 was used as follows

$$K_d = \frac{(C_b/C_a - 1) \times V}{w} \qquad (2)$$

where C_b and C_a are the elemental concentrations in ppm in the solution before and after equilibration, respectively, w is the weight of dry AG50W-X8 resin in grams, and V is the volume of acid solution in mL. The distribution coefficients are given in Table 2 and Figure 1 (base-10 logarithmic scale). For a given concentration, a high K_d value means that the element is preferentially retained on the resin, while a low K_d indicates the release of the element to the mobile phase. Only values within the range $10 < K_d < 10^{4.5}$ are considered reliable in this study, because below 10, insufficient change in the solution concentrations occur, while above $10^{4.5}$, solution concentrations approach the detection limits of the MC−ICPMS.

For all 19 elements investigated, the distribution coefficients decrease with increasing α-HIBA molarity (Figure 1). For the REEs, a negative linear relationship is observed between distribution coefficients and α-HIBA molarity in a log−log space. As α-HIBA forms stronger complexes with heavier REEs,[79] at a given molarity, lighter REEs have higher K_d than heavier REEs, and elution occurs in decreasing order of atomic numbers.[73,80] Table 3 gives the linear regression statistics for each element, and the best-fit lines are shown in Figure 2. Slopes, intercepts, and the goodness of fits are determined using the LINEST function in Microsoft Excel. R^2 values on these regressions range from 0.987 to 0.998. The equations include a pH term, to account for K_d variations as a function of the α-HIBA solution pH (see below).

3.2. Accounting for pH Variations. The mobile phase pH can significantly influence the K_d values of REEs for the α-HIBA chemistry.[58,81] Indeed, as a weak monobasic acid, the dissociation of α-HIBA is described by the chemical reaction

$$[\text{HIBA}] \leftrightarrow [\text{H}^+] + [\text{L}^-] \qquad (3)$$

https://dx.doi.org/10.1021/acsearthspacechem.0c00273
ACS Earth Space Chem. 2021, 5, 55−65

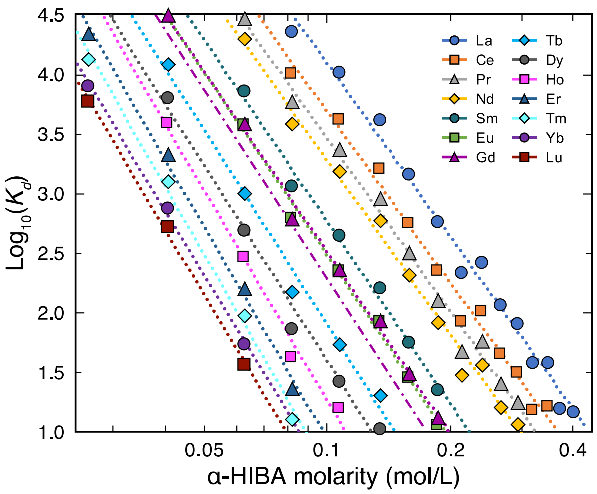

Figure 2. Distribution coefficients of REEs on AG50W-X8 resin in logarithmic scale as a function of α-HIBA molarity. Dotted lines show linear regressions using partition coefficients between 10 and $10^{4.5}$ (see equations in Table 3). The dotted-dashed line represents the corrected distribution coefficients of Gd (see text for details).

where L represents the ligand of α-HIBA. Through the dissociation constant of this reaction, the ligand concentration can thus be expressed as

$$[L^-] = \frac{K_a[HIBA]}{[H^+]} \quad (4)$$

or in log form, as

$$pL = -\log_{10}([L^-]) = pK_a - pH - \log_{10}([HIBA]) \quad (5)$$

This relationship is well known, and for instance, Deelstra and Verbeek[58] showed that the $\log_{10}(K_d)$ of the REEs was linearly related to pL. At constant pH, the ligand concentration (which determines the value of the partition distribution, K_ds) is only a function of the α-HIBA molarity (see Figure 2).

As shown by eq 5, changes in ligand concentration can be similarly produced by variations in α-HIBA molarity or pH. Although the K_d values reported here were obtained at constant pH (=4.50), these values can be adjusted to account for changes in pH by equating them to the change in molarity that would be needed to maintain a constant ligand concentration. For instance, if the pH of α-HIBA solution is changed by ΔpH, the following relationship can be written as follows

$$pL = pK_a - (pH + \Delta pH) - (\log_{10}([HIBA]) - \Delta pH) \quad (6)$$

A pH change of magnitude $+\Delta$pH is therefore equivalent to a change in log α-HIBA molarity of magnitude $-\Delta$pH. For any α-HIBA molarity, the appropriate K_d values at different pH values can simply read on Figure 2 by moving horizontally by $-\Delta$pH (relative to the pH = 4.50). Mathematically, this means modifying the intercepts of the linear regression equations in Table 3 by a value $m \times \Delta$pH (where m is the slope of regression lines). In Table 3, we present general formulas accounting for pH difference relative to the calibration pH of 4.50.

4. DISCUSSION

4.1. Correction of the Gd Distribution Coefficients.

Unlike other REEs, the distribution coefficients of Gd and Eu obtained from the batch experiments overlap. If correct, this would indicate that both elements should elute together during the α-HIBA chemistry, which conflicts with observations in previous studies.[58,59,61−65,82−84] The apparently higher distribution coefficients measured for Gd are very likely due to $^{141}Pr^{16}O$ interferences. At a given α-HIBA molarity, the distribution coefficient of Pr is always larger than that of Gd. Hence, the impact of the PrO interference on Gd in the nonequilibrated solution is larger than in the equilibrated solution, leading to systematically higher K_d values for Gd. Using a quartz spray chamber for sample introduction into the MC−ICPMS (as was done here) typically produces several to several tens of percent of Pr oxide, which significantly affects the determination of Gd K_d values (Supporting Information). This effect was, unfortunately, not precisely quantified during mass spectrometric analysis. However, a correction of the Gd K_d values is possible when considering the K_d values across all REEs.

To first-order, electrostatics controls REE partitioning on the cation-exchange resin. Elements with smaller ionic radii and higher charge densities are expected to be surrounded by larger hydration spheres, which in turn decreases the surface charge density and the affinity for the resin (*i.e.*, hydrated radius decreases with increasing ionic radius and *vice versa*).[85] Accordingly, $\log_{10}(K_d)$ should thus depend linearly on the reciprocal of the ionic radius.[31] Figure 3 shows the slope (a) and

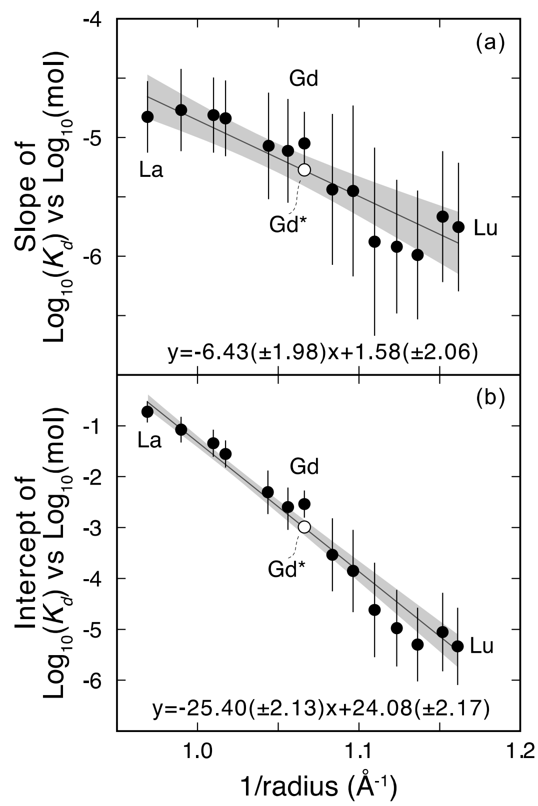

Figure 3. Slope (a) and intercept (b) of the linear regressions, as shown in Figure 2, as a function of the reciprocal of ionic radii.[86] The open symbol denotes Gd* (see text for details).

intercept (b) of the $\log_{10}(K_d)$ versus $\log_{10}([HIBA])$ best-fit lines for all REEs, plotted against the reciprocal of the ionic radius (radii from ref 86). Both the slope and the intercept of the best-fit lines are linearly correlated to the reciprocal of the ionic radius. Interestingly, Gd falls off the 95% CI of the intercept versus $1/r$ correlation defined by the other REEs (Figure 3b). It

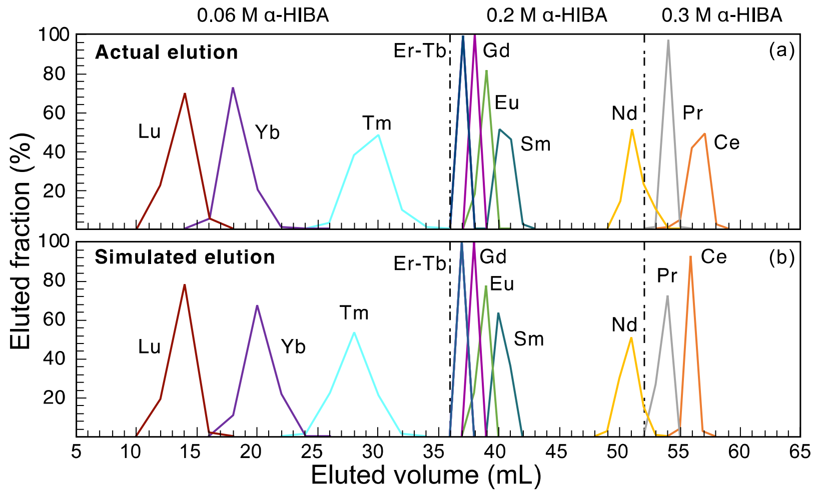

Figure 4. (a) Experimental elution profile of REEs using a gravity-driven quartz column: 1.9 mm ID × 21 cm length. Condition: AG50W-X8 resin (200−400 mesh) with α-HIBA (pH = 4.50), at room temperature (∼22 °C). (b) Simulated elution profile, assuming: resin porosity, 49%;[88] density of the extractant-loaded beads, 0.70 g/mL; (HETP = 0.50 ± 0.20 mm).

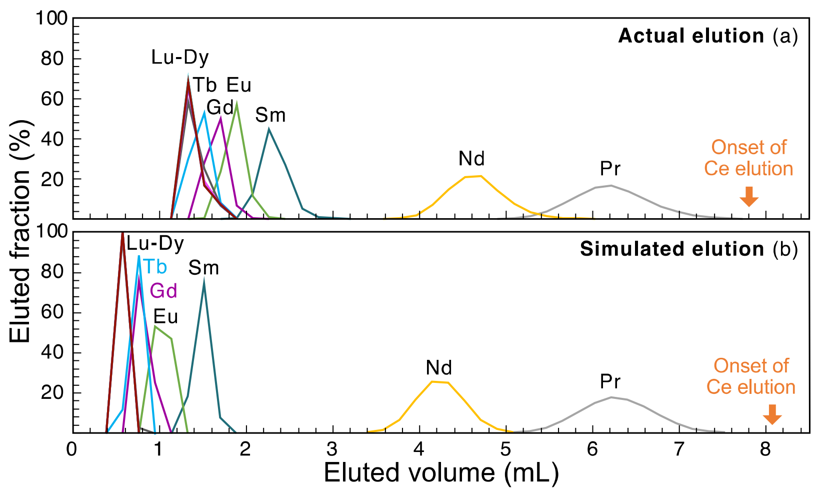

Figure 5. (a) Experimental elution profile of REEs using a pressurized (1.0 psi) borosilicate column (2.0 mm ID × 30 cm length), with AG50W-X4 resin (200−400 mesh) and α-HIBA (pH = 4.62), at room temperature (∼22 °C). The resulting flow rate was 47 μL/min. (b) Simulated elution profile, assuming: resin porosity, 57%;[88] density of the extractant-loaded beads, 0.70 g/mL; (HETP = 1.5 ± 0.2 mm).

is also slightly offset from (although within uncertainty of) the correlation defined by other REEs in the slope versus $1/r$ space (Figure 3a). By bringing Gd on the regression lines defined by other REEs in Figure 3a,b, we obtain a new value of the slope and intercept of the $\log_{10}(K_d)$ versus $\log_{10}([\text{HIBA}])$ best-fit line, referred to in Tables 2 and 3 as Gd*. We will show below that the corrected values for Gd* accurately predict the position of the Gd peak in our elution tests, and therefore, we recommend use of the corrected Gd* values.

4.2. Comparison of Actual and Simulated Elution Curves. To avoid potentially unsuccessful and time-consuming elution tests when trying to optimize a separation protocol, an efficient approach consists in using a computational chromatography code to simulate the elution results. Knowledge of the distribution coefficients of the elements of interest in each elution step is, however, a prerequisite to perform such simulations. To test the reliability of the distribution coefficients obtained in this study, we carried out simulations to try and reproduce two elutions using different column sizes and experimental setups. The accuracy and applicability of the K_d reported here are assessed by inspecting the consistency of the simulated and actual elution curves.

Elution 1: a gravity-driven separation of most REEs was conducted using a custom-made quartz column (see Figure 4 and Section 2.5), and the simulated results are shown in Figure 4b. While the K_d values calculated using the regression, as shown in Table 3, mainly impact peak position, the HETP mainly controls peak width and was determined to be 0.50 ± 0.20 mm (by adjusting the value of the HETP to fit the actual elution profile). Overall, the simulation successfully reproduces the actual elution. To perfectly match the heavy REE peak position, the α-HIBA molarity of the first elution step had to be very slightly adjusted, from the 0.060 M value used in the actual elution to 0.058 M. This slight (3.3%) discrepancy likely stems for the imprecision associated with the preparation of such a dilute α-HIBA solution (during the batch experiment and/or the elution).

Elution 2: as the α-HIBA chemistry is widely used for Nd purification for high-precision isotope analysis,[10,18,32,34,66,67,70−72] our second comparison aimed at testing the usefulness of the reported K_d values when predicting fine-

https://dx.doi.org/10.1021/acsearthspacechem.0c00273
ACS Earth Space Chem. 2021, 5, 55−65

scale separations (*i.e.*, drop-by-drop), even under slightly different experimental conditions than those used for the K_d determinations. We conducted an isocratic elution with 0.2 M α-HIBA on AG50W-X4 (200−400 mesh) at pH = 4.62 (Figure 5a). The resin cross-linkage and eluent pH were different from those used for K_d determination, providing an adequate challenge to test the reliability of our data and methods for correcting pH effects. Given that both pH and resin cross-linkage can influence the distribution coefficients,[61,81,87] a perfect match between the actual elution (X4 resin, pH = 4.62) and simulated elution (X8 resin, pH = 4.50) was not expected and was not obtained, even when accounting for the pH difference as explained in Section 3.2. Indeed, the light REEs eluted too late in the simulation, consistent with the general tendency of K_d values to increase with higher cross-linkage.[80] Adjusting the eluent molarity to 0.213 M (6.5% higher than the actual α-HIBA molarity used) in Figure 5b produces an exact match for the position of the Pr peak. The HETP was found to be 1.5 ± 0.2 mm. At this molarity, the peak positions of Nd and Ce are also satisfactorily matched. While Sm and the heavier REEs are predicted to elute too early, we note that the K_d values of these elements at this molarity were below the detection limit of the batch equilibration experiments, and we are thus working beyond the validity domain of the best-fit lines used to predict the K_d values (Table 3). The small (6.5%) adjustment in molarity accounts for the combined impact of all systematic biases (resin cross-linkage, eluent molarity offsets, and other experimental conditions such as T), which are only resolvable owing to the drop-by-drop (*i.e.*, fine-scale) nature of the elution.

Overall, this test shows that direct optimization of fine-scale (*i.e.*, drop-by-drop) REE elution cannot rely solely on the K_d values reported herein, but that systematic adjustment of these K_d values can produce reliable elution curves over the domain of validity of the best-fit lines provided in Table 3. For practical purposes of fine-scale elutions, conducting a preliminary elution is necessary in order to assess the systematic offset of K_d values between this study and the actual experimental setup. Equipped with such a first elution, the intercepts of the best-fit lines (Table 3) in $\log_{10}(K_d)$ versus $HIBA_{molarity}$ space can be modified to anchor the K_d values to the specific experimental setup. After such recalibration, the newly adjusted distribution coefficients can be utilized to guide the fine-scale optimization of the elution scheme.

5. SUMMARY

Batch equilibration experiments were performed to determine the distribution coefficients of the REEs, Sr, Y, Ba, Th, and U on the AG50W-X8 resin (200−400 mesh size) in α-HIBA solution over a wide range of molarity. For REEs, the distribution coefficients are found to decrease linearly with increasing α-HIBA molarity (in log−log space). The accuracy of the distribution coefficients was tested based on their capacity to reproduce two elution curves obtained using different experimental setups. The good agreement between the actual elution profiles and simulated results demonstrates the accuracy of the K_d values reported herein, which can therefore be used to design novel separation schemes of REEs or optimizing existing ones.

■ ASSOCIATED CONTENT

Supporting Information

The Supporting Information is available free of charge at https://pubs.acs.org/doi/10.1021/acsearthspacechem.0c00273.

Estimation of $^{141}Pr^{16}O$ interference on ^{157}Gd; architecture of the chromatography simulation code; results of simulated elution obtained using various column dimensions; results of simulated elution obtained using various resin properties; and 95% confidence intervals of best-fit linear regression lines for determination of REE K_d as a function of α-HIBA molarity (PDF)

Simulation Code Package including guide to the elution simulation code; Chromatography_Simulation_2.3 (Mathematica notebook); Input template; input example; and input output example (ZIP)

■ AUTHOR INFORMATION

Corresponding Author

François L. H. Tissot − *The Isotoparium, Division of Geological and Planetary Sciences, California Institute of Technology, Pasadena 91125-0002, California, United States; Origins Laboratory, Department of the Geophysical Sciences and Enrico Fermi Institute, The University of Chicago, Chicago 60637, Illinois, United States;* orcid.org/0000-0001-6622-2907; Email: tissot@caltech.edu

Authors

Haoyu Li − *The Isotoparium, Division of Geological and Planetary Sciences, California Institute of Technology, Pasadena 91125-0002, California, United States;* orcid.org/0000-0002-7192-2470

Seung-Gu Lee − *Origins Laboratory, Department of the Geophysical Sciences and Enrico Fermi Institute, The University of Chicago, Chicago 60637, Illinois, United States; Geological Research Division, Korea Institute of Geoscience and Mineral Resources, Daejeon 34132, Republic of Korea*

Eugenia Hyung − *The Isotoparium, Division of Geological and Planetary Sciences, California Institute of Technology, Pasadena 91125-0002, California, United States*

Nicolas Dauphas − *Origins Laboratory, Department of the Geophysical Sciences and Enrico Fermi Institute, The University of Chicago, Chicago 60637, Illinois, United States*

Complete contact information is available at: https://pubs.acs.org/10.1021/acsearthspacechem.0c00273

Author Contributions

N.D., F.L.H.T., and S-G.L. conceived the study. S.-G.L. and F.L.H.T. performed the partitioning experiments. H.L. and F.L.H.T. processed and interpreted the data. E.H. conducted Elution 2. H.L. wrote the first draft under F.L.H.T.'s guidance. All authors contributed to writing and/or editing of the manuscript.

Notes

The authors declare no competing financial interest.

■ ACKNOWLEDGMENTS

We thank the three anonymous reviewers and editor Joel D. Blum for constructive criticisms, which greatly helped us to improve the manuscript. This work was supported by grants NASA grants NNX17AE86G, NNX17AE87G, 80NSSC17K0744, and 80NSSC20K0821 and NSF grant

EAR-2001098 to N.D.; grant GP2020-003 (provided by Korea Institute of Geoscience and Mineral Resources) to S.-G.L.; NASA grant 80NSSC20K1398 (PI: F.L.H.T., FI: H.L.), NSF grant EAR-1824002, and start-up funds (provided by Caltech) to F.L.H.T.

REFERENCES

(1) Caro, G.; Bourdon, B.; Birck, J.-L.; Moorbath, S. ^{146}Sm-^{142}Nd Evidence from Isua Metamorphosed Sediments for Early Differentiation of the Earth's Mantle. *Nature* **2003**, *423*, 428−432.

(2) Boyet, M.; Carlson, R. W. ^{142}Nd Evidence for Early (>4.53 Ga) Global Differentiation of the Silicate Earth. *Science* **2005**, *309*, 576−581.

(3) Burkhardt, C.; Borg, L. E.; Brennecka, G. A.; Shollenberger, Q. R.; Dauphas, N.; Kleine, T. A Nucleosynthetic Origin for the Earth's Anomalous ^{142}Nd Composition. *Nature* **2016**, *537*, 394−398.

(4) Bouvier, A.; Boyet, M. Primitive Solar System Materials and Earth Share a Common Initial ^{142}Nd Abundance. *Nature* **2016**, *537*, 399−402.

(5) Shollenberger, Q. R.; Brennecka, G. A. Dy, Er, and Yb Isotope Compositions of Meteorites and Their Components: Constraints on Presolar Carriers of the Rare Earth Elements. *Earth Planet. Sci. Lett.* **2020**, *529*, 115866.

(6) Saji, N. S.; Wielandt, D.; Holst, J. C.; Bizzarro, M. Solar System Nd Isotope Heterogeneity: Insights into Nucleosynthetic Components and Protoplanetary Disk Evolution. *Geochim. Cosmochim. Acta* **2020**, *281*, 135.

(7) Andreasen, R.; Sharma, M. Solar Nebula Heterogeneity in P-Process Samarium and Neodymium Isotopes. *Science* **2006**, *314*, 806−809.

(8) Andreasen, R.; Sharma, M. Mixing and Homogenization in the Early Solar System: Clues from Sr, Ba, Nd, and Sm Isotopes in Meteorites. *Astrophys. J.* **2007**, *665*, 874−883.

(9) Bennett, V. C.; Brandon, A. D.; Nutman, A. P. Coupled ^{142}Nd-^{143}Nd Isotopic Evidence for Hadean Mantle Dynamics. *Science* **2007**, *318*, 1907−1910.

(10) Carlson, R. W.; Boyet, M.; Horan, M. Chondrite Barium, Neodymium, and Samarium Isotopic Heterogeneity and Early Earth Differentiation. *Science* **2007**, *316*, 1175−1178.

(11) O'Neil, J.; Carlson, R. W.; Francis, D.; Stevenson, R. K. Neodymium-142 Evidence for Hadean Mafic Crust. *Science* **2008**, *321*, 1828−1831.

(12) Thrane, K.; Connelly, J. N.; Bizzarro, M.; Meyer, B. S.; The, L.-S. Origin of Excess ^{176}Hf in Meteorites. *Astrophys. J.* **2010**, *717*, 861−867.

(13) Gannoun, A.; Boyet, M.; Rizo, H.; El Goresy, A. ^{146}Sm-^{142}Nd Systematics Measured in Enstatite Chondrites Reveals a Heterogeneous Distribution of ^{142}Nd in the Solar Nebula. *Proc. Natl. Acad. Sci. U.S.A.* **2011**, *108*, 7693−7697.

(14) Albalat, E.; Telouk, P.; Albarède, F. Er and Yb Isotope Fractionation in Planetary Materials. *Earth Planet. Sci. Lett.* **2012**, *355−356*, 39−50.

(15) Faure, G.; Mensing, T. M. *Isotopes: Principles and Applications*; Wiley, 2005.

(16) Friedman, A. M.; Milsted, J.; Metta, D.; Henderson, D.; Lerner, J.; Harkness, A. L.; Rok Op, D. J. Alpha Decay Half Lives of ^{148}Gd ^{150}Gd and ^{146}Sm. *Radiochim. Acta* **1966**, *5*, 192.

(17) Li, S.; Jagoutz, E.; Chen, Y.; Li, Q. Sm−Nd and Rb−Sr Isotopic Chronology and Cooling History of Ultrahigh Pressure Metamorphic Rocks and Their Country Rocks at Shuanghe in the Dabie Mountains, Central China. *Geochim. Cosmochim. Acta* **2000**, *64*, 1077−1093.

(18) Marks, N. E.; Borg, L. E.; Hutcheon, I. D.; Jacobsen, B.; Clayton, R. N. Samarium-Neodymium Chronology and Rubidium-Strontium Systematics of an Allende Calcium-Aluminum-Rich Inclusion with Implications for ^{146}Sm Half-Life. *Earth Planet. Sci. Lett.* **2014**, *405*, 15−24.

(19) White, W. M.; Hofmann, A. W. Sr and Nd Isotope Geochemistry of Oceanic Basalts and Mantle Evolution. *Nature* **1982**, *296*, 821−825.

(20) Blichert-Toft, J.; Puchtel, I. S. Depleted Mantle Sources through Time: Evidence from Lu−Hf and Sm−Nd Isotope Systematics of Archean Komatiites. *Earth Planet. Sci. Lett.* **2010**, *297*, 598−606.

(21) Blichert-Toft, J.; Boyet, M.; Télouk, P.; Albarède, F. ^{147}Sm−^{143}Nd and ^{176}Lu−^{176}Hf in Eucrites and the Differentiation of the HED Parent Body. *Earth Planet. Sci. Lett.* **2002**, *204*, 167−181.

(22) Bouvier, A.; Vervoort, J. D.; Patchett, P. J. The Lu−Hf and Sm−Nd Isotopic Composition of CHUR: Constraints from Unequilibrated Chondrites and Implications for the Bulk Composition of Terrestrial Planets. *Earth Planet. Sci. Lett.* **2008**, *273*, 48−57.

(23) Caro, G.; Bourdon, B.; Birck, J.-L.; Moorbath, S. High-Precision ^{142}Nd/^{144}Nd Measurements in Terrestrial Rocks: Constraints on the Early Differentiation of the Earth's Mantle. *Geochim. Cosmochim. Acta* **2006**, *70*, 164−191.

(24) Render, J.; Fischer-Gödde, M.; Burkhardt, C.; Kleine, T. The Cosmic Molybdenum-Neodymium Isotope Correlation and the Building Material of the Earth. *Geochem. Persp. Let.* **2017**, *3*, 170−178.

(25) Segal, I.; Halicz, L.; Platzner, I. T. Accurate Isotope Ratio Measurements of Ytterbium by Multiple Collection Inductively Coupled Plasma Mass Spectrometry Applying Erbium and Hafnium in an Improved Double External Normalization Procedure. *J. Anal. At. Spectrom.* **2003**, *18*, 1217−1223.

(26) Willig, M.; Stracke, A. Accurate and Precise Measurement of Ce Isotope Ratios by Thermal Ionization Mass Spectrometry (TIMS). *Chem. Geol.* **2018**, *476*, 119−129.

(27) Lee, S.-G.; Tanaka, T. Determination of Eu Isotopic Ratio by Multi-Collector Inductively Coupled Plasma Mass Spectrometry Using a Sm Internal Standard. *Spectrochim. Acta, Part B* **2019**, *156*, 42−50.

(28) Pourkhorsandi, H.; Debaille, V.; de Jong, J.; Armytage, R. M. G. Cerium Stable Isotope Analysis of Synthetic and Terrestrial Rock Reference Materials by MC-ICPMS. *Talanta* **2020**, DOI: 10.1016/j.talanta.2020.121877.

(29) Willig, M.; Stracke, A. Earth's Chondritic Light Rare Earth Element Composition: Evidence from the Ce−Nd Isotope Systematics of Chondrites and Oceanic Basalts. *Earth Planet. Sci. Lett.* **2019**, *509*, 55−65.

(30) Hu, J. Y.; Dauphas, N.; Tissot, F. L. H.; Yokochi, R.; Ireland, T. J.; Zhang, J. Z.; Davis, A. M.; Ciesla, F. J.; Grossman, L.; Charlier, B. L. A.; Alp, E. E.; Hu, M. Y.; Zhao, J. Major heating events in the nascent solar system recorded by rare earth element isotopic fractionation in refractory inclusions. *Sci. Adv.*, **2021**, in press.

(31) Nash, K. L.; Jensen, M. P. Analytical-Scale Separations of the Lanthanides: A Review of Techniques and Fundamentals. *Sep. Sci. Technol.* **2001**, *36*, 1257−1282.

(32) Lugmair, G. W.; Scheinin, N. B.; Marti, K. Sm-Nd Age and History of Apollo 17 Basalt 75075-Evidence for Early Differentiation of the Lunar Exterior. *Lunar and Planetary Science Conference Proceedings*; 1975; Vol. *6*, pp 1419−1429.

(33) Depaolo, D. J.; Wasserburg, G. J. Nd Isotopic Variations and Petrogenetic Models. *Geophys. Res. Lett.* **1976**, *3*, 249−252.

(34) Jacobsen, S. B.; Wasserburg, G. J. Sm-Nd Isotopic Evolution of Chondrites. *Earth Planet. Sci. Lett.* **1980**, *50*, 139−155.

(35) Wasserburg, G. J.; Jacobsen, S. B.; DePaolo, D. J.; McCulloch, M. T.; Wen, T. Precise Determination of Sm/Nd Ratios, Sm and Nd Isotopic Abundances in Standard Solutions. *Geochim. Cosmochim. Acta* **1981**, *45*, 2311−2323.

(36) Jacobsen, S. B.; Wasserburg, G. J. Sm-Nd Isotopic Evolution of Chondrites and Achondrites, II. *Earth Planet. Sci. Lett.* **1984**, *67*, 137−150.

(37) Rehkämper, M.; Gärtner, M.; Galer, S. J. G.; Goldstein, S. L. Separation of Ce from Other Rare-Earth Elements with Application to Sm-Nd and La-Ce Chronometry. *Chem. Geol.* **1996**, *129*, 201−208.

(38) Debaille, V.; Brandon, A. D.; Yin, Q. Z.; Jacobsen, B. Coupled ^{142}Nd−^{143}Nd Evidence for a Protracted Magma Ocean in Mars. *Nature* **2007**, *450*, 525−528.

(39) Caro, G.; Bourdon, B.; Halliday, A. N.; Quitté, G. Super-Chondritic Sm/Nd Ratios in Mars, the Earth and the Moon. *Nature* **2008**, *452*, 336−339.

(40) Patchett, P. J.; Tatsumoto, M. A Routine High-Precision Method for Lu-Hf Isotope Geochemistry and Chronology. *Contrib. Mineral. Petrol.* **1981**, *75*, 263−267.
(41) Blichert-Toft, J.; Chauvel, C.; Albarède, F. Separation of Hf and Lu for High-Precision Isotope Analysis of Rock Samples by Magnetic Sector-Multiple Collector ICP-MS. *Contrib. Mineral. Petrol.* **1997**, *127*, 248−260.
(42) Münker, C.; Weyer, S.; Scherer, E.; Mezger, K. Separation of High Field Strength Elements (Nb, Ta, Zr, Hf) and Lu from Rock Samples for MC-ICPMS Measurements. *Geochem., Geophys., Geosyst.* **2001**, *2*, 1064.
(43) Yang, Y.-h.; Zhang, H.-f.; Chu, Z.-y.; Xie, L.-w.; Wu, F.-y. Combined Chemical Separation of Lu, Hf, Rb, Sr, Sm and Nd from a Single Rock Digest and Precise and Accurate Isotope Determinations of Lu-Hf, Rb-Sr and Sm-Nd Isotope Systems Using Multi-Collector ICP-MS and TIMS. *Int. J. Mass Spectrom.* **2010**, *290*, 120−126.
(44) Pin, C.; Gannoun, A. Integrated Extraction Chromatographic Separation of the Lithophile Elements Involved in Long-Lived Radiogenic Isotope Systems (Rb-Sr, U-Th-Pb, Sm-Nd, La-Ce, and Lu-Hf) Useful in Geochemical and Environmental Sciences. *Anal. Chem.* **2017**, *89*, 2411−2417.
(45) Tanaka, T.; Masuda, A. The La−Ce Geochronometer: A New Dating Method. *Nature* **1982**, *300*, 515−518.
(46) Tanaka, T.; Shimizu, H.; Kawata, Y.; Masuda, A. Combined La−Ce and Sm−Nd Isotope Systematics in Petrogenetic Studies. *Nature* **1987**, *327*, 113−117.
(47) Shimizu, H.; Umemoto, N.; Masuda, A.; Appel, P. W. U. Sources of Iron-Formations in the Archean Isua and Malene Supracrustals, West Greenland: Evidence from La-Ce and Sm-Nd Isotopic Data and REE Abundances. *Geochim. Cosmochim. Acta* **1990**, *54*, 1147−1154.
(48) Makishima, A.; Nakamura, E. Precise Measurement of Cerium Isotope Composition in Rock Samples. *Chem. Geol.* **1991**, *94*, 1−11.
(49) Hayashi, T.; Tanimizu, M.; Tanaka, T. Origin of Negative Ce Anomalies in Barberton Sedimentary Rocks, Deduced from La−Ce and Sm−Nd Isotope Systematics. *Precambrian Res.* **2004**, *135*, 345−357.
(50) Hidaka, H.; Ebihara, M.; Shima, M. Determination of the Isotopic Compositions of Samarium and Gadolinium by Thermal Ionization Mass Spectrometry. *Anal. Chem.* **1995**, *67*, 1437−1441.
(51) Hidaka, H.; Ebihara, M.; Yoneda, S. High Fluences of Neutrons Determined from Sm and Gd Isotopic Compositions in Aubrites. *Earth Planet. Sci. Lett.* **1999**, *173*, 41−51.
(52) Sands, D. G.; De Laeter, J. R.; Rosman, K. J. R. Measurements of Neutron Capture Effects on Cd, Sm and Gd in Lunar Samples with Implications for the Neutron Energy Spectrum. *Earth Planet. Sci. Lett.* **2001**, *186*, 335−346.
(53) Leya, I.; Wieler, R.; Halliday, A. N. The Influence of Cosmic-Ray Production on Extinct Nuclide Systems. *Geochim. Cosmochim. Acta* **2003**, *67*, 529−541.
(54) Hidaka, H.; Yoneda, S.; Nishiizumi, K. Cosmic-Ray Exposure Histories of Martian Meteorites Studied from Neutron Capture Reactions of Sm and Gd Isotopes. *Earth Planet. Sci. Lett.* **2009**, *288*, 564−571.
(55) Choppin, G. R.; Silva, R. J. Separation of the Lanthanides by Ion Exchange with Alpha-Hydroxy Isobutyric Acid. *J. Inorg. Nucl. Chem.* **1956**, *3*, 153−154.
(56) Smith, H. L.; Hoffman, D. C. Ion-Exchange Separations of the Lanthanides and Actinides by Elution with Ammonium Alpha-Hydroxy-Isobutyrate. *J. Inorg. Nucl. Chem.* **1956**, *3*, 243−247.
(57) Choppin, G. R.; Chopoorian, J. A. Complexes of the Lanthanide Elements with α-Hydroxy Carboxylate Ligands. *J. Inorg. Nucl. Chem.* **1961**, *22*, 97−113.
(58) Deelstra, H.; Verbeek, F. The Separation of the Lanthanides and Yttrium by Cation Exchange Elution with Ammonium α-Hydroxyisobutyrate and Lactate. *J. Chromatogr. A* **1965**, *17*, 558−566.
(59) Massart, D. L.; Bossaert, W. The Prediction of Elution Maxima in the Gradient Elution of Rare Earths. *J. Chromatogr. A* **1968**, *32*, 195−200.
(60) Eugster, O.; Tera, F.; Burnett, D. S.; Wasserburg, G. J. Isotopic Composition of Gadolinium and Neutron-Capture Effects in Some Meteorites. *J. Geophys. Res.* **1970**, *75*, 2753−2768.
(61) Sisson, D. H.; Mode, V. A.; Campbell, D. O. High-Speed Separation of the Rare Earths by Ion Exchange Part II. *J. Chromatogr. A* **1972**, *66*, 129−135.
(62) Campbell, D. O. Rapid Rare Earth Separation by Pressurized Ion Exchange Chromatography. *J. Inorg. Nucl. Chem.* **1973**, *35*, 3911−3919.
(63) Story, J.; Fritz, J. Forced-Flow Chromatography of the Lanthanides with Continuous in-Stream Detection. *Talanta* **1974**, *21*, 892−894.
(64) Campbell, D. O. Separation of Lanthanides and Trivalent Actinides with Pressurized Ion Exchange. *Sep. Purif. Methods* **1976**, *5*, 97−138.
(65) Qaim, S. M.; Ollig, H.; Blessing, G. Separation of Lanthanides by Preparative High Pressure Liquid Chromatography. *Radiochim. Acta* **1979**, *26*, 59−62.
(66) Amakawa, H.; Ingri, J.; Masuda, A.; Shimizu, H. Isotopic Compositions of Ce, Nd and Sr in Ferromanganese Nodules from the Pacific and Atlantic Oceans, the Baltic and Barents Seas, and the Gulf of Bothnia. *Earth Planet. Sci. Lett.* **1991**, *105*, 554−565.
(67) Borg, L. E.; Nyquist, L. E.; Taylor, L. A.; Wiesmann, H.; Shih, C.-Y. Constraints on Martian Differentiation Processes from Rb-Sr and Sm-Nd Isotopic Analyses of the Basaltic Shergottite QUE 94201. *Geochim. Cosmochim. Acta* **1997**, *61*, 4915−4931.
(68) Meisel, T.; Schöner, N.; Paliulionyte, V.; Kahr, E. Determination of Rare Earth Elements, Y, Th, Zr, Hf, Nb and Ta in Geological Reference Materials G-2, G-3, SCo-1 and WGB-1 by Sodium Peroxide Sintering and Inductively Coupled Plasma-mass Spectrometry. *Geostand. Newsl.* **2002**, *26*, 53−61.
(69) Harvey, J.; Baxter, E. F. An Improved Method for TIMS High Precision Neodymium Isotope Analysis of Very Small Aliquots (1−10 Ng). *Chem. Geol.* **2009**, *258*, 251−257.
(70) Rizo, H.; Boyet, M.; Blichert-Toft, J.; Rosing, M. Combined Nd and Hf Isotope Evidence for Deep-Seated Source of Isua Lavas. *Earth Planet. Sci. Lett.* **2011**, *312*, 267−279.
(71) Garçon, M.; Boyet, M.; Carlson, R. W.; Horan, M. F.; Auclair, D.; Mock, T. D. Factors Influencing the Precision and Accuracy of Nd Isotope Measurements by Thermal Ionization Mass Spectrometry. *Chem. Geol.* **2018**, *476*, 493−514.
(72) Hyung, E.; Jacobsen, S. B. The $^{142}Nd/^{144}Nd$ Variations in Mantle-Derived Rocks Provide Constraints on the Stirring Rate of the Mantle from the Hadean to the Present. *Proc. Natl. Acad. Sci. U.S.A.* **2020**, *117*, 14738−14744.
(73) Fuping, H.; Haddad, P. R.; Jackson, P. E.; Carnevale, J. Studies on the Retention Behaviour of α-Hydroxyisobutyric Acid Complexes of Thorium(IV) and Uranyl Ion in Reversed-Phase High-Performance Liquid Chromatography. *J. Chromatogr. A* **1993**, *640*, 187−194.
(74) Strelow, F. W. E. Quantitative Separation of Lanthanides and Scandium from Barium, Strontium and Other Elements by Cation-Exchange Chromatography in Nitric Acid. *Anal. Chim. Acta* **1980**, *120*, 249−254.
(75) Pourmand, A.; Dauphas, N. Distribution Coefficients of 60 Elements on TODGA Resin: Application to Ca, Lu, Hf, U and Th Isotope Geochemistry. *Talanta* **2010**, *81*, 741−753.
(76) Pourmand, A.; Dauphas, N.; Ireland, T. J. A Novel Extraction Chromatography and MC-ICP-MS Technique for Rapid Analysis of REE, Sc and Y: Revising CI-Chondrite and Post-Archean Australian Shale (PAAS) Abundances. *Chem. Geol.* **2012**, *291*, 38−54.
(77) Ireland, T. J.; Tissot, F. L. H.; Yokochi, R.; Dauphas, N. Teflon-HPLC: A Novel Chromatographic System for Application to Isotope Geochemistry and Other Industries. *Chem. Geol.* **2013**, *357*, 203−214.
(78) Martin, A. J. P.; Synge, R. L. M. A New Form of Chromatogram Employing Two Liquid Phases: A Theory of Chromatography. 2. Application to the Micro-Determination of the Higher Monoamino-Acids in Proteins. *Biochem. J.* **1941**, *35*, 1358.
(79) Sivaraman, N.; Kumar, R.; Subramaniam, S.; Vasudeva Rao, P. R. Separation of Lanthanides Using Ion-Interaction Chromatography with

HDEHP Coated Columns. *J. Radioanal. Nucl. Chem.* **2002**, *252*, 491−495.

(80) Barkley, D. J.; Blanchette, M.; Cassidy, R. M.; Elchuk, S. Dynamic Chromatographic Systems for the Determination of Rare Earths and Thorium in Samples from Uranium Ore Refining Processes. *Anal. Chem.* **1986**, *58*, 2222−2226.

(81) Pourjavid, M. R.; Norouzi, P.; Ganjali, M. R. Light Lanthanides Determination by Fast Fourier Transform Continuous Cyclic Voltammetry after Separation by Ion-Exchange Chromatography. *Int. J. Electrochem. Sci.* **2009**, *4*, 923−942.

(82) Matsui, M.; Aoki, T.; Kumagai, T. Forced-Flow Chromatography of Rare Earths Using Sensitive Spectrophotometry (Commemoration Issue Dedicated to Professor Megumi Tashiro on the Occation of His Retirement). *Bull. Inst. Chem. Res.* **1981**, *59*, 207.

(83) Garcia-Valls, R.; Hrdlicka, A.; Perutka, J.; Havel, J.; Deorkar, N. V.; Tavlarides, L. L.; Muñoz, M.; Valiente, M. Separation of Rare Earth Elements by High Performance Liquid Chromatography Using a Covalent Modified Silica Gel Column. *Anal. Chim. Acta* **2001**, *439*, 247−253.

(84) Raut, N. M.; Jaison, P. G.; Aggarwal, S. K. Separation and Determination of Lanthanides, Thorium and Uranium Using a Dual Gradient in Reversed-Phase Liquid Chromatography. *J. Chromatogr. A* **2004**, *1052*, 131−136.

(85) Korkisch, J. *CRC Handbook of Ion Exchange Resins*; CRC Press, 1988; Vol. *6*.

(86) Shannon, R. D. Revised Effective Ionic Radii and Systematic Studies of Interatomic Distances in Halides and Chalcogenides. *Acta Crystallogr., Sect. A: Cryst. Phys., Diffr., Theor. Gen. Crystallogr.* **1976**, *32*, 751−767.

(87) Walt, T. N. v. d.; Strelow, F. W. E.; Verheij, R. The Influence Of Crosslinkage On The Distribution Coefficients And Anion Exchange Behaviour Of Some Elements In Hydrochloric Acid. *Solvent Extr. Ion Exch.* **1985**, *3*, 723−740.

(88) Lee, S. C.; Hsiang, C. C.; Huang, H.; Ting, G. A Comparative Study of Gel-Type and Macroreticular Cation Exchange Resins for the Separation of Rare Earth Elements. *Sep. Sci. Technol.* **1990**, *25*, 1857−1870.

https://dx.doi.org/10.1021/acsearthspacechem.0c00273
ACS Earth Space Chem. 2021, 5, 55−65